Blade imbalance fault identification in doubly fed induction generator through current signature analysis using wavelet transform

Vivek Kushwaha[1], Arvind Kumar Yadav[2], Sanjay Kumar Maurya[2]
[1]Department of Electrical Engineering, Gyan Ganga Institute of Technology and Sciences, Jabalpur, India
[2]Department of Electrical Engineering, GLA University, Mathura, India

ABSTRACT

Using wind turbines (WTs) equipped with doubly fed induction generators (DFIG) is a popular technology for generating renewable energy. To ensure safe operation, prompt maintenance, and better operational reliability, the induction generator used in wind energy must be monitored. In this paper, an analysis is carried out on stator currents of the DFIG machine in a wind farm to identify any blade imbalances in the wind farm. A fault characteristics extraction analysis is carried out on the machine stator currents to detect the fault in the system. Firstly, the mathematical equation of the DFIG blade unbalanced stator current is generated using the DFIG model. Secondly, Park's Transformation is used to modify the stator's 3-phase current. Further, by evaluating the feature frequency amplitude variation in the squared signal by doing a spectral analysis on the stator current vector's squared signal. Lastly, a Simulink model for the DFIG is developed. The suggested approach analyses the fault signal of the imbalanced blade fault at various wind velocities. The outcomes show that the suggested method for diagnosing impeller imbalance faults can successfully locate the fault.

This is an open access article under the CC BY-SA license.

Corresponding Author:

Vivek Kushwaha
Department of Electrical Engineering, Gyan Ganga Institute of Technology and Sciences
Jabalpur, Madhya Pradesh, India
Email: vivekkushwaha@ggits.org

1. INTRODUCTION

Early fault diagnosis reduces machine failure by 75%. Timely fault identification is crucial for reliable wind turbine (WT) operation. Fault diagnosis tech is critical in power and energy generation by making it more dependable. The marine current turbine's rotor blade pitch imbalance defect is proposed in [1]. Continuous Morlet wavelet transform and K-nearest neighbour (KNN) machine learning are used to classify fault severity in fault diagnosis. MRnet, a novel technique, utilizes photos taken by automated aerial vehicles to identify blade defects in WTs. Mask region-based convolutional neural network (R-CNN) and MRnet networks are used for fault detection, segmentation, and classification. proposes a methodology for frequency control of microgrids using droop control in the generator-side converter (GSC) with battery energy storage system (BESS) [2]. The spatiotemporal distribution of natural wind speed and the effects of wind shear and tower shadow effect are analyzed along with blade mass imbalance fault in DFIG WTs [3]. Frequency spectrum and Lissajous curves are studied and analysed to detect WTs flaws [4]. Zhang *et al*. [5] proposes an image array for recognizing the defect in turbine blades using a neural network. Finally, it diagnoses faults in the field-oriented control of doubly fed induction generators (DFIG) using frequency spectrum and Lissajous curves [6].

Han *et al*. [7] combined the unstable streamlined and WT dynamic models to compute a unique response based on beam theory in a typhoon for 6 MW and 2 MW WTs. Meanwhile, Rolán and Pedra [8] proposed a calculation to investigate DFIG WT. At the same time [9] highlighted the need for a geographic information system and presented an improved condition monitoring system, and [10] used a parameter estimation technique and an observer approach to diagnose mechanical drive train faults in WTs.

The use of the artificial neural network (ANN) in WTs is analyzed [11]. The study outlines the main challenges and technology gaps. Another study [12], highlights how an inter-turn short circuit (ITSC) fault can impact the performance of an induction generator in WTs. The effect of increasing the power converter switching frequency of DFIG during fault conditions is investigated [13]. To improve the fault ride-through (FRT) capability of DFIG, the switching frequency control parallel resonance fault current limiter (SFC-PRFCL) is applied. Additionally, Shohag *et al*. [14] reviews the various types of damage that WT blades can experience and the preventive measures. Lastly, a novel multi-level inverter is developed in [15] to protect the DFIG from voltage drops caused by power system issues.

Zhao *et al*. [16], discuss WT impeller mass moment computation under five different circumstances. Hichem and Tahar [17] presents fuzzy logic for fault monitoring and identification. Yang and Chai [18] is a review of fault diagnostics research for wind converters. Qiao and Lu [19] presents a comprehensive review of condition monitoring and fault identification methods for offshore WTs. Patel and Patel [20] presents a complete study on WT's transient stability. Mishra and Shaikh [21] presents a model for simulating steady-state behaviours of a DFIG.

The researchers [22]–[24] respectively report on rotor unbalance, acoustic emission detection method, and PQ theory for permanent magnet synchronous generators. Kusiak and Verma [25] analyses data-mining algorithms using data from a large wind farm. An algorithm is introduced that restructures mass and aerodynamic imbalances by [26]. Amirat *et al*. [27] describes a tool for detecting bearing issues and the stator current signal.

DFIG WTs have different faults such as gearbox faults, blade imbalance faults, and interturn faults. The most common fault is the blade imbalance fault. It is necessary to identify these faults early for the reliability of the system. Various techniques are applied to identify these faults such as KNN, ANN, CNN, and MRnet. The power spectral density method and the order tracking analysis method are proposed for detecting imbalance faults by analyzing aerodynamic torque [28]. The spatiotemporal distribution of natural wind speed and the effects of wind shear and tower shadow effect are analyzed along with blade mass imbalance fault in DFIG WTs [3].

In this paper, an analysis is done on stator currents of the DFIG WT to identify any blade imbalance conditions in the wind farm. The results of spectrum analysis and the various wavelet decomposition components of the signals show the abnormalities of the signal with the blade imbalance fault. Whenever the wind speed exceeds its critical limit, the amplitude characteristic frequency $I_0^2(t)$ is also exceeded. The defect characterization methodology is used to monitor the changes in the magnitude of the characteristic frequency $I_0^2(t)$ under the same wind speed condition to identify the severity of impeller imbalance flaws. This analysis is carried out with the variable wind speed which changes with respect to the real time. To validate the results, wavelet analysis is carried out on the flow of the reactive power of DFIG to determine the disturbances in the signal during healthy and faulty conditions. A DFIG Simulink model with blade imbalance is developed in this study using stator current characteristic analysis and its coordinate transformation. Additional stator currents are evaluated in comparison to their spectrum. The fault characteristic component of the characteristic frequency magnitude, $I_0(t)$, grows as the wind speed increases. By keeping track of variations in the stator current fault characteristic component's characteristic frequency amplitude under the same wind speed conditions, the component may accurately assess the sternness of the blade imbalance fault.

2. DOUBLY FED INDUCTION GENERATOR

Nowadays modern power electronics converters control the rotor currents in the DFIG to achieve the variable speed necessary to maximize energy from the variable wind. Figure 1 depicts the standard non-uniform velocity WT system with a DFIG. Rotor turbine blades, a gearbox, a generator, and a power electronics converter are the main components of the DFIG machine. Research by Hammouchi *et al*. [6] GSC, DC link, and rotor-side converter (RSC) are the components that make up the power converter module. The common connection is used to couple the stator, GSC, and DFIG to the grid. The dynamic equations of DFIG in d-q components applying the Park transformation are given in accordance with the motor sign convention and the synchronous reference frame.

$$V_{sd} = (R_s + L_s p)i_{sd} + Mpi_{rd} - L_s \omega_s i_{sq} - M\omega_s i_{rq} \qquad (1)$$

$$V_{sq} = (R_s + L_s p)i_{sq} + Mpi_{rq} - L_s \omega_s i_{sd} - M\omega_s i_{rd} \qquad (2)$$

$$V_{rd} = (R_r + L_r p)i_{rd} + Mpi_{sd} - L_r s\omega_s i_{rq} - Ms\omega_s i_{sq} \tag{3}$$

$$V_{rq} = (R_r + L_r p)i_{rq} + Mpi_{sq} - L_r s\omega_s i_{rd} - Ms\omega_s i_{sd} \tag{4}$$

$$\Gamma_m = \wp M(i_{rd}i_{sq} - i_{rq}i_{sd} \tag{5}$$

where V_{sd} is stator voltage direct component, V_{sq} is stator voltage quadrature component, V_{rd} is rotor voltage direct component, V_{rq} is rotor voltage quadrature component, I_{sd} is stator current direct component, I_{sq} is stator current quadrature component, I_{rd} is rotor current direct component, I_{rq} is rotor current quadrature component, R_s is stator winding resistance, R_r is rotor winding resistance, L_s is stator winding reactance, L_r is rotor winding reactance, and p is d/dt is the first order derivative operator.
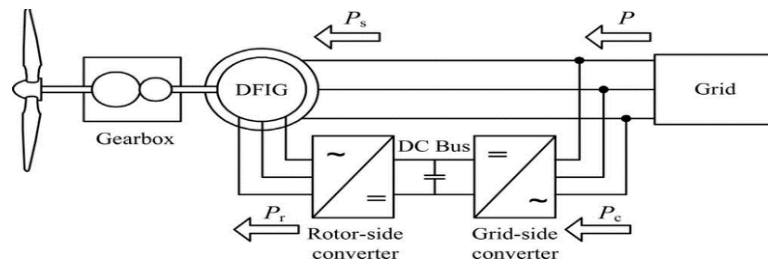

Figure 1. Considering the motor sign convention, DFIG-based WT with active powers representation

Γm shows electro-magnetic torque, d and q are the direct and quadrature components of the Park transformation respectively; and s represents stator and r represents rotor. s=(ωs−℘ ωm)/ωs is the DFIG slip. Figure 2 shows equivalent circuits that can be used to depict dynamic equations of DFIG.
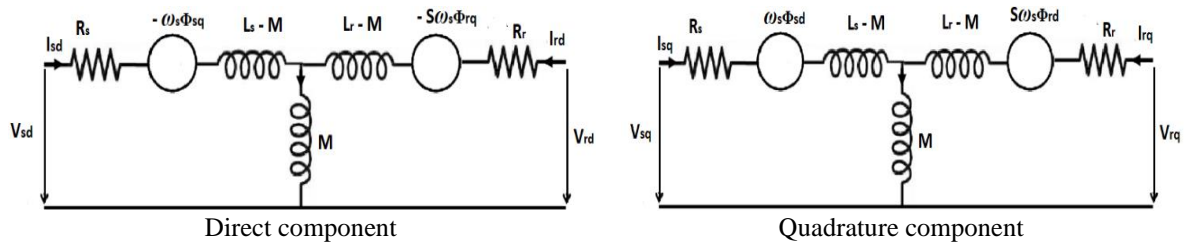Where: φsd=Ls isd, φsq=Ls isq, φrd=Lr ird, and φrq=Lr irq.

Figure 2. DFIG equivalent circuit with d-q components

The instantaneous value of active and reactive power that is switched amongst the grid and the WT is given as:

$$p = p_s + p_c = V_{sd}i_{sd} + V_{sq}i_{sd} - V_{rd}i_{rd} + V_{rq}i_{rq}$$

$$q = q_s + q_r = V_{sd}i_{sd} + V_{sq}i_{sd}$$

Where the converter's power losses are disregarded, i.e., $p_c = p_r$ and the GSC is expected to be operate with unity power factor, i.e., $q_r = 0$.

3. MATHEMATICAL MODELLING FOR BLADE IMBALANCE FAILURE'S EFFECT ON THE STATOR CURRENT OF A WT

When a WT has three blades and is run at a fixed angular speed of m (rad/s), the blade imbalance fault can be said to be present in terms of shaft torque.

$$T = T_0 + T_v \sin(\omega_m t + \phi) \tag{6}$$

Here t(s) is time; T (Nm) is WT shaft, output torque; T_0 (Nm) is aerodynamic torque; T_v (Nm) is fluctuation torque due to blade imbalance fault; and ϕ(rad) is early phase angle.

With its wheels, drive shaft, gearbox, and generator rotor, the DFIG transmission mechanism was equivalent to a centred mass symbolised by:

$$2H_M \frac{d\omega_m}{dt} = T - T_e - D_M \omega_m \tag{7}$$

Here H_M is equivalent inertia time constant; T_e(N·m) is electromagnetic torque; and D_M, damping coefficient~0, at a steady condition, $d\omega_m/dt=0$.

In (6) and (7), show the electromagnetic torque oscillates at the same frequency as the shaft torque's cyclic oscillation. Consequently, the electromagnetic torque can be explained as follows when the blade is unbalanced:

$$T_e = T_{e0} + T_{ev} \sin(\omega_m t + \phi) \tag{8}$$

Here T_{e0} (Nm) is electromagnetic torque established by the related aerodynamic torque T_0 (Nm) and T_{ev} (Nm) is electromagnetic torque formed by the equivalent imbalance torque T_v (Nm).

The isq component in the q-axis direction of the stator current can also be used to express the electromagnetic torque Te (Nm):

$$T_e = \frac{3p}{2} = \Psi_s i_{sq} \tag{9}$$

Where p is No. of pole and s(Wb) is stator winding flux linkages.

From (10) can be calculated using the DFIG stator flux orientation model:

$$\frac{d\Psi_{sd}}{dt} = -R_s i_{sd} + u_{sd}$$
$$\sigma L_s \frac{di_{sd}}{dt} = -\frac{L_s R_r + L_r R_s}{dt} i_{sd} + \frac{R_r \Psi_{sd}}{L_r} \sigma L_s \omega_s i_{sq} + u_{sd} \tag{10}$$
$$\sigma = 1 - \frac{L_m^2}{L_s L_r}$$

where s_d is stator flux s, d-axis component, i_{sd} is stator current i_s, u_{sd} is stator voltage u_s, R_s and R_r is stator and rotor resistance, respectively, L_s and L_r is stator and rotor inductance, respectively, L_m is magnetizing inductance, and ω_s is slip angular velocity.

To obtain Ψ_{sd} in the steady state operation of the WT, we need eliminate the u_{sd} in (10).

$$\Psi_{sd} = L_s i_{sd} - \sigma \frac{L_r}{R_r} L_s \omega_s i_{sq} \tag{11}$$

From the stator flux orientation model, the Ψ_{sq} that is the q-axis direction component of the stator flux Ψ_s is equal to 0. Thus,

$$\Psi_s = \Psi_{sd} = L_s i_{sd} - \sigma \frac{L_r}{R_r} L_s \omega_s i_{sq} \tag{12}$$

In the steady state case, the stator flux Ψ_s is constant. The periodic oscillation in Te causes the q-axis component of stator current i_{sq} to have the same vibration frequency. Thus:

$$i_{sq} = i_{sq0} + A_{siq} \sin(\omega_m t + \phi_q) \tag{13}$$

Similarly, when combined with the stator flux Ψ_s expression in (12), the d-axis component of stator current i_{sd} also shows the same vibration frequency, as (14):

$$i_{sd} = i_{sd0} + A_{sid} \sin(\omega_m t + \phi_q) \tag{14}$$

In (13) and (14), the stator current components i_{sq0} and i_{sd0} are generated by T_0, respectively. A_{sid} and A_{siq} are the amplitudes of the additional stator currents generated by the imbalanced torque T_v, which are proportional to T_{ev}. ϕ_d and ϕ_q are the initial phase angles of the current i_{sd} and i_{sq}, respectively.

The stator current can be transformed from the *dq* coordinate system to the *abc* three-phase coordinate system when combined with the *dq-abc* transformation, the calculated *a* phase stator current is as (15):

$$i_{sa}(t) = i_0 \sin(\omega_e t + \phi_0)$$
$$+ \frac{1}{2}\{A_{sid}\cos[(\omega_e + \omega_m)t - \phi_d] + A_{siq}\cos[(\omega_e - \omega_m)t - \phi_q]\} \tag{15}$$
$$- \frac{1}{2}\{A_{sid}\cos[(\omega_e + \omega_m)t + \phi_d] - A_{siq}\cos[(\omega_e - \omega_m)t + \phi_q]\}$$

where $i_0 = \sqrt{i_{sd0}^2 + i_{sq0}^2}$, ϕ_0 is arctan (i_{sq0}/i_{sd0}), and ω_e is the synchronous rotation angular velocity. Usually, $\phi_d \approx \phi_q$, (15) can be simplified further as (16):

$$i_{sa}(t) = i_0 \sin(\omega_e t + \phi_0) + A_1\cos[(\omega_e - \omega_m)t - \phi_d] + A_{siq}\cos[(\omega_e + \omega_m)t - \phi_q] \tag{16}$$

Where $A_1 = \frac{A_{siq} + A_{sid}}{2}$ and $A_2 = \frac{A_{siq} - A_{sid}}{2}$

In (16) indicates that the blade imbalance would cause the DFIG stator current to produce a harmonic component with frequency $f e \pm f m$ ($\omega e=2 \pi f$ e, $\omega m=2 \pi f m$) (Hz). Although the harmonic component can theoretically be utilized to diagnose blade imbalance failure, the actual fault's effect on the harmonic component's amplitude is typically minimal. Thus, base frequency current leakage and outside noise can readily drown out the amplitude.

3.1. Method used for doubly fed induction generators system analysis

Spectrum analysis detects errors by identifying changes in the amplitude of the featured frequency of the squared signal stator current vector. To extract fault characteristics, a feature extraction technique using Park transform, wavelet and spectrum analysis is intended. Blade imbalance results in harmonic components with a characteristic frequency of $f e \pm f m$ in the stator current. Direct spectral analysis cannot extract fault characteristics. Coordinate transformation can analyze stator-phase current fault characteristics successfully at consistent and tempestuous wind velocities. Wavelet and spectrum analysis can diagnose blade unbalance. See Figure 3 for the steps.
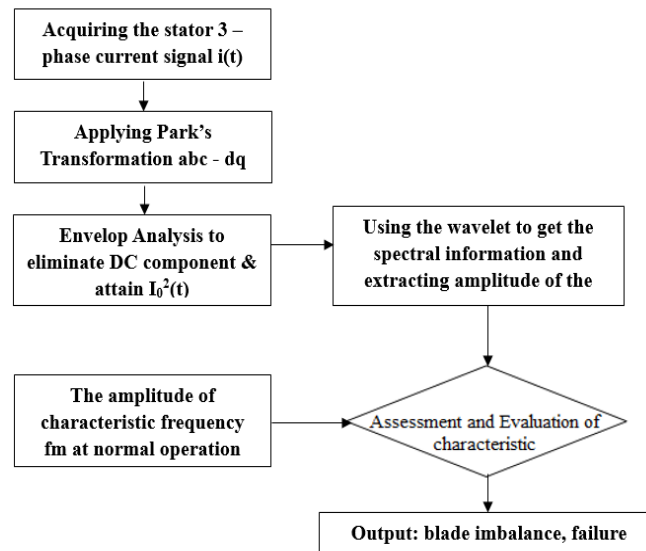

Figure 3. Flow chart for fault diagnosis of DFIG WT

4.   RESULT ANALYSIS

Utilizing Simulink, a DFIG simulation model with per-unit values and a blade imbalance condition is created. This model validates the effectiveness of the suggested approach for the stator current fault analysis. Park's transformation methodology is applied to determine the impeller imbalance faults in the DFIG.

The block diagram model is presented in Figure 4. This block diagram consists of a 3-phase source, a transmission line of 30 km, and a step-down transformer which is directly coupled with the DFIG WT. The dq-axis components as well as the fault characteristic component with fm frequency of the DFIG stator current can be observed through the scope under the normal and blade imbalance fault conditions.
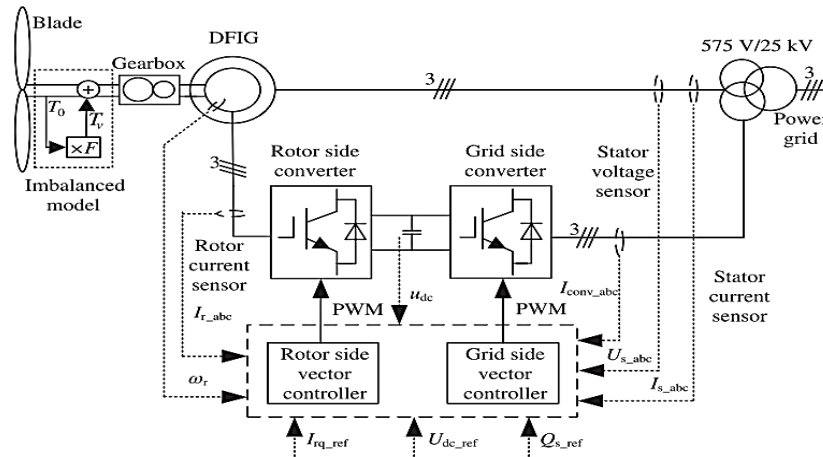
Figure 4. Simulation model

4.1. Characteristic analysis of stator-phase current fault

Direct spectrum analysis on stator current and turbine speed shows that transforming the 3-phase stator current from 3-d to 2-d coordinates using Park's transformation can accurately identify fault characteristic frequency, even at high wind velocities, and can successfully detect blade:

$$i_\alpha = \sqrt{\frac{2}{3}} i_a - \sqrt{\frac{1}{6}} i_b - \sqrt{\frac{1}{6}} i_c$$

$$i_\beta = \sqrt{\frac{1}{2}} i_b - \sqrt{\frac{1}{2}} i_c$$

$$I^2(t) = i_\alpha^2 + i_\beta^2$$

Park's transformation and the squared signal $I^2(t)$ is used to convert the DFIG stator 3-phase current i(t) into two-dimensional space. Park's transformation's main idea is to translate the 3-phase stator current into 2-D coordinates. Using envelope analysis to obtain the upper and lower envelopes of $I^2(t)$. By removing the DC component:

$$I_0^2(t) = I^2(t) - [I_{dup}^2(t) + I_{down}^2(t)]/2$$

The frequency of the fault feature amplitude can be determined by doing spectral analysis shown in Figure 5. By contrasting the feature frequency amplitude with the variation in the feature frequency magnitude during normal action, the savagery of the blade imbalance fault may be assessed.
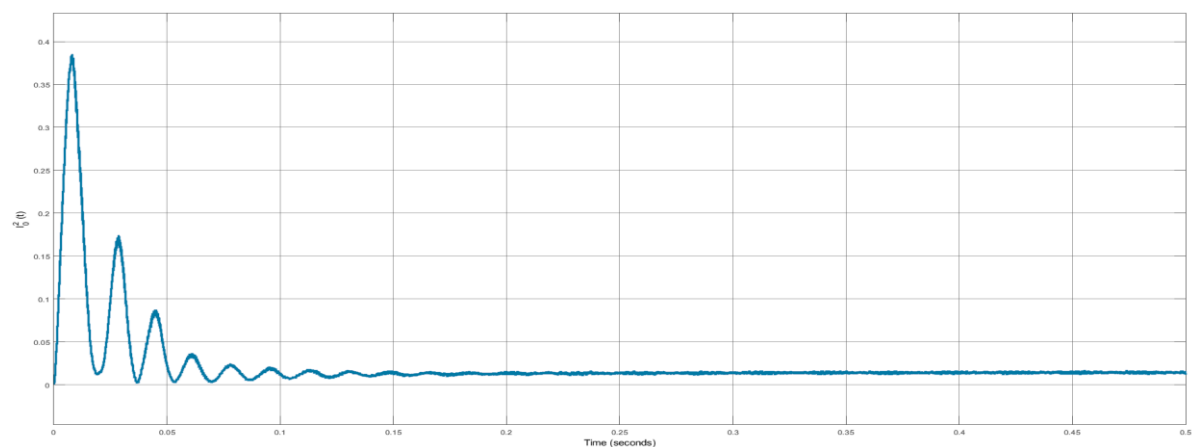

Figure 5. Stator current fault characterization analysis

4.2. Characteristic analysis of stator-phase current fault

The characteristics of DFIG under normal condition is shown in the Figure 6. The 3-phase p.u. voltage at 575 V bus, 3 phase p.u. current through 575 V bus, and flow of real and reactive power shown in Figures 6(a)-(d) respectively. From the obtained results it is analyzed that DFIG operates under blade balance conditions. Further, Figures 6(e)-(h) show DC excitation voltage, rotor speed in p.u., and the 3 phase p.u. voltage at 25 kV bus, 3 phase p.u. current through 25 kV bus respectively. These results validate the normal operating condition of DFIG.
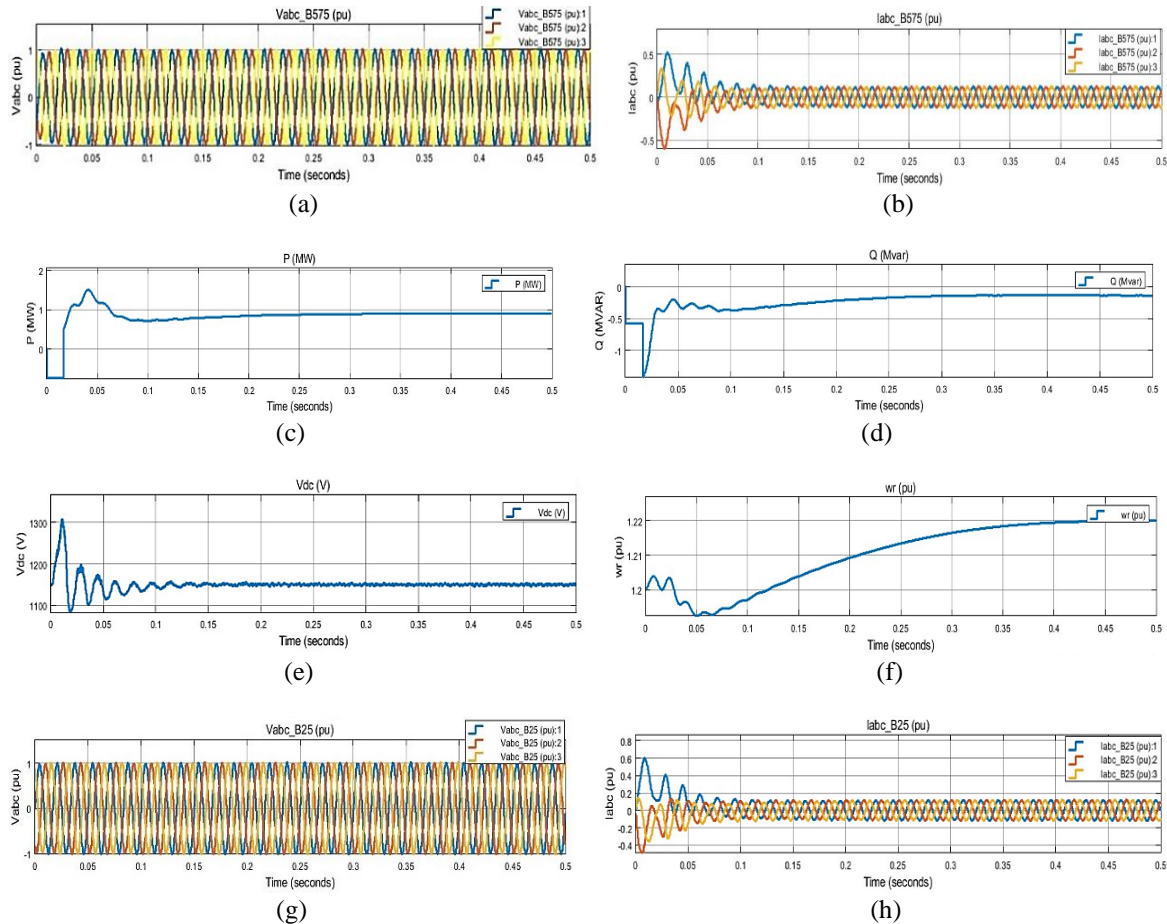

(a)

(b)

(c)

(d)

(e)

(f)

(g)

(h)

Figure 6. The characteristics of DFIG under normal condition; (a) 3-phase p.u. voltage of DFIG at 575 V bus under normal condition, (b) 3-phase p.u. current of DFIG at 575 V bus under normal condition, (c) 3-phase active power under normal condition, (d) 3-phase reactive power under normal condition, (e) DC voltage of DFIG under normal condition, (f) rotor speed under normal condition, (g) 3-phase p.u. voltage of DFIG at 25 kV bus under normal condition, and (h) 3-phase p.u. current of DFIG at 25 kV bus under normal condition

To investigate blade imbalance in a DFIG WT, a fault was simulated by changing the pitch angle of the blades at 0.4 seconds. The resulting characteristics are shown in Figure 7. A comparison was made between the normal and imbalance conditions. Due to blade imbalance condition various changes are observed in the results are described in Figure 7.

The 3-phase p.u. voltage at 575 V bus, 3 phase p.u. current through 575 V bus, and flow of real and reactive power shown in Figures 7(a)-(d) respectively. From the obtained results it is analyzed that DFIG operates under blade balance conditions. Further, Figures 7(e)-(h) are shows DC excitation voltage, rotor speed in p.u., and the 3 phase p.u. voltage at 25 kV bus, 3 phase p.u. current through 25 kV bus respectively. These results validate the normal operating condition of DFIG.
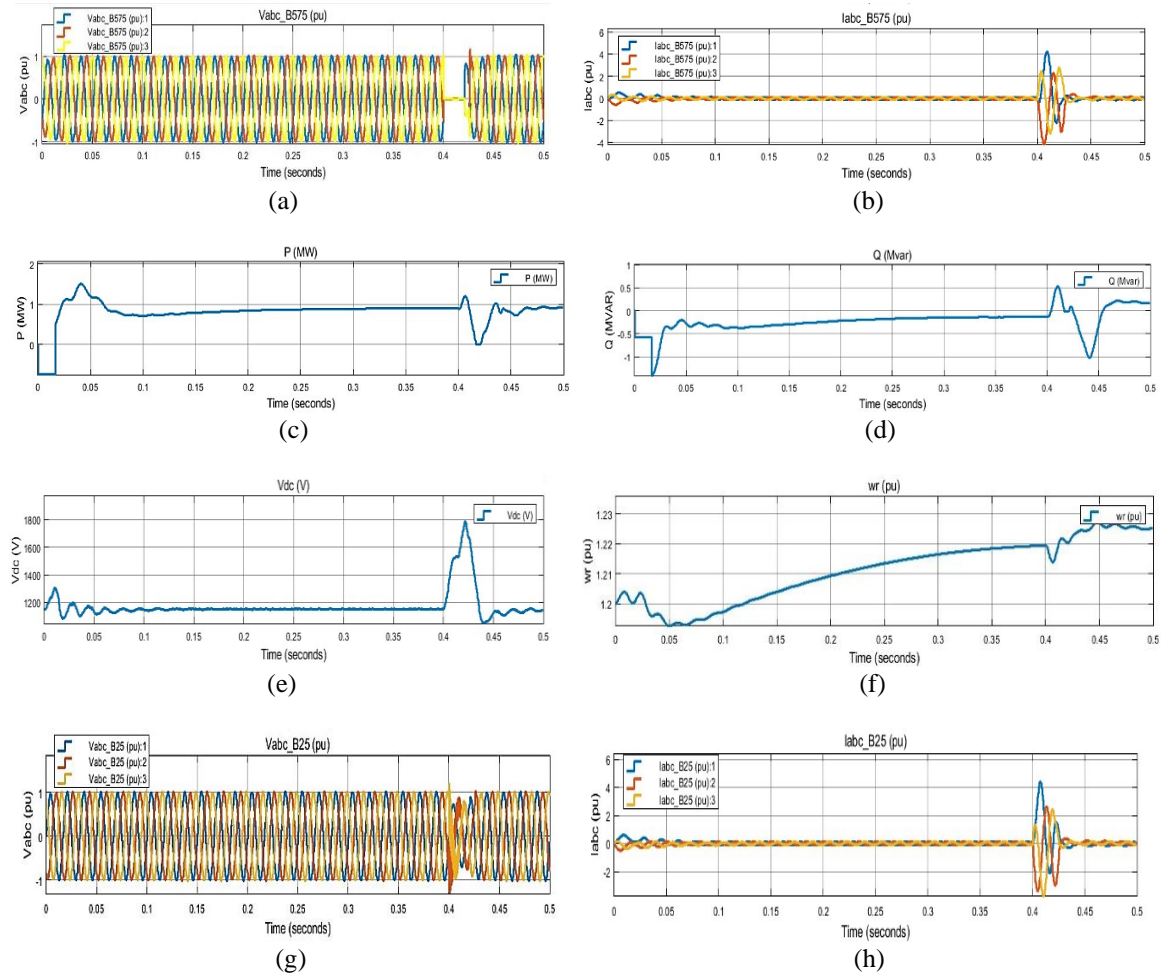
Figure 7. The characteristics of DFIG under blade imbalace condition; (a) 3-phase p.u. voltage of DFIG at 575 V bus under fault, (b) 3-phase p.u. current of DFIG at 575 V bus under fault, (c) 3-phase active power under fault, (d) 3-phase reactive power under fault, (e) DC voltage of DFIG under fault, (f) rotor speed under fault, (g) 3-phase p.u. voltage of DFIG at 25 kV bus under fault, and (h) 3-phase p.u. current of DFIG at 25 kV bus under fault

4.3. Wavelet analysis

Figures 8 and 9 are display both the original signal and its respective wavelet coefficients. Multilevel wavelet decomposition is carried out to divide the signal into two components: approximation coefficients and detailed coefficients. Single-level wavelet decomposition divides the signal into low-pass (approximation) components and high-pass (detailed) components. After the first level of decomposition, the approximation coefficients are obtained and further decomposed to result in second-level approximation coefficients (a2) and detailed coefficients (d2). This process is repeated for a total of 5 levels of decomposition, resulting in the coefficients d1, d2, d3, d4, d5, and a5.

The wavelet analysis was carried out successfully and showed the waveform of the reactive power flow in the DFIG under healthy conditions. The waveforms in Figure 8 consist of various components of the reactive power absorbed by the DFIG, which validates its steady state. Next, the wavelet analysis was carried out with a fault introduced at 0.4 seconds. The waveform in Figure 9 shows the flow of reactive power in the DFIG with the fault. The various components of the reactive power consumed by the DFIG are shown with changes in amplitudes at 0.4 seconds, which validates the faulty state of the DFIG. To effectively assess the severity of the blade imbalance fault, it is expected that fluctuations in the amplitude component of the fault characteristic frequency of the stator current will be possible under the same wind speed conditions. Therefore, by comparing the variation in the frequency amplitude feature of $I_0^2(t)$ with that in normal operation, it is possible to measure the severity of the blade imbalance defect.
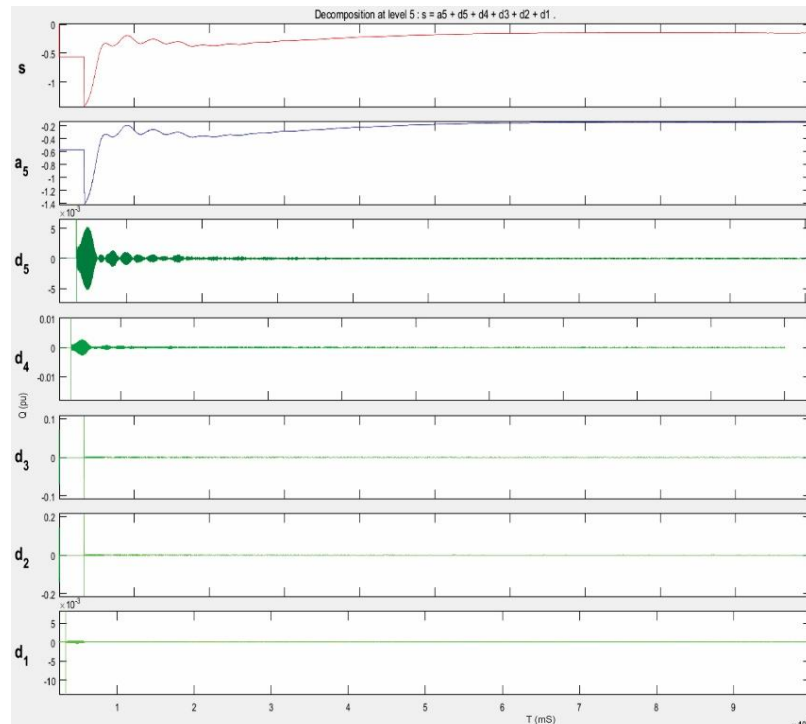
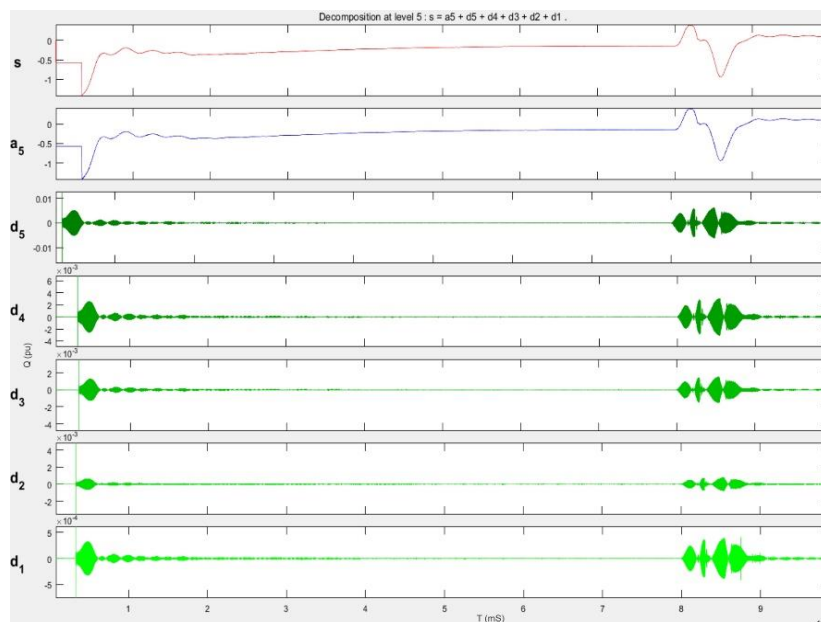Figure 8. Reactive power analysis of DFIG under normal condition

Figure 9. Reactive power analysis of DFIG under fault

5. CONCLUSION

This study analyses stator currents of a DFIG WT to identify blade imbalance conditions in the wind farm. The defect characterization methodology monitors the characteristic frequency $I_0^2(t)$ to identify the severity of impeller imbalance flaws in real time, while wavelet analysis validates the results. The proposed approach analyses stator current characteristic extracts and diagnoses impeller imbalance failure in both steady-state and turbulent wind conditions. This method can accurately assess the severity of the blade imbalance fault by tracking variations in the stator current fault characteristic component's characteristic frequency amplitude under the same wind speed conditions.

REFERENCES

[1]   B. Freeman, Y. Tang, Y. Huang, and J. VanZwieten, "Rotor blade imbalance fault detection for variable-speed marine current turbines via generator power signal analysis," *Ocean Eng.*, vol. 223, 2021, doi: 10.1016/j.oceaneng.2021.108666.

[2]   L. A. G. Gomez, A. P. Grilo, M. B. C. Salles, and A. J. S. Filho, "Combined control of DFIG-based wind turbine and battery energy storage system for frequency response in microgrids," *Energies*, vol. 13, no. 4, 2020, doi: 10.3390/en13040894.

[3]   S. Wan, K. Cheng, X. Sheng, and X. Wang, "Characteristic Analysis of DFIG Wind Turbine under Blade Mass Imbalance Fault in View of Wind Speed Spatiotemporal Distribution," *Energies*, vol. 12, no. 16, p. 3178, Aug. 2019, doi: 10.3390/en12163178.

[4]   F. El Hammouchi, L. El Menzhi, and A. Saad, "DFIG defects diagnosis method for wind energy conversion chain," *Adv. Sci. Technol. Eng. Syst.*, vol. 4, no. 5, pp. 174–185, 2019, doi: 10.25046/aj040523.

[5]   N. Zhang, C. Lu, and A. Wang, "Study on wind turbine blade defect detection system based on imaging array," *E3S Web Conf.*, vol. 118, pp. 3–6, 2019, doi: 10.1051/e3sconf/201911802041.

[6]   F. El Hammouchi, L. El Menzhi, and A. Saad, "Diagnosis Method for Wind Turbine Doubly Fed Induction Generator under Grid Defects," vol. 3, no. 3, pp. 46–55, 2019.

[7]   R. Han, L. Wang, T. Wang, Z. Gao, and J. Wu, "Study of dynamic response characteristics of the wind turbine based on measured power spectrum in the eyewall region of typhoons," *Appl. Sci.*, vol. 9, no. 12, 2019, doi: 10.3390/app9122392.

[8]   A. Rolán and J. Pedra, "Initialization of DFIG wind turbines with a phasor-based approach," *Wind Energy*, vol. 22, no. 3, pp. 420–432, Mar. 2019, doi: 10.1002/we.2296.

[9]   J. Shen, "Classification of Wind Turbine Blade Performance State Through Statistical Methods," 2019.

[10] S. Asgari and A. Yazdizadeh, *Robust model-based fault diagnosis of mechanical drive train in V47/660 kW wind turbine*, vol. 9, no. 4. Springer Berlin Heidelberg, 2018. doi: 10.1007/s12667-017-0231-2.

[11] A. P. Marugán, F. P. G. Márquez, J. M. P. Perez, and D. Ruiz-Hernández, "A survey of artificial neural network in wind energy systems," *Appl. Energy*, vol. 228, pp. 1822–1836, 2018, doi: 10.1016/j.apenergy.2018.07.084.

[12] T. Sellami, H. Berriri, S. Jelassi, A. M. Darcherif, and M. F. Mimouni, "Performance analysis of grid-connected wind turbine system under Inter-Turn Short-Circuit fault conditions," *Int. J. Renew. Energy Res.*, vol. 8, no. 1, pp. 374–383, 2018.

[13] M. R. Islam and M. R. I. Sheikh, "Transient stability enhancement of DFIG based wind generator by switching frequency control strategy with parallel resonance fault current limiter," *Glob. J. Res. Eng.*, vol. 18, no. 1, pp. 39–48, 2018.

[14] M. A. S. Shohag, E. C. Hammel, D. O. Olawale, and O. I. Okoli, "Damage mitigation techniques in wind turbine blades: A review," *Wind Eng.*, vol. 41, no. 3, pp. 185–210, 2017, doi: 10.1177/0309524X17706862.

[15] A. D. Falehi and M. Rafiee, "Enhancement of DFIG-Wind Turbine's LVRT capability using novel DVR based Odd-nary Cascaded Asymmetric Multi-Level Inverter," *Eng. Sci. Technol. an Int. J.*, vol. 20, no. 3, pp. 805–824, 2017, doi: 10.1016/j.jestch.2017.05.004.

[16] P. Zhao, X. Li, and L. Yang, "Research on Mass Imbalance Fault of Wind Turbine Based on Virtual Prototype," *MATEC Web Conf.*, vol. 95, pp. 0–5, 2017, doi: 10.1051/matecconf/20179506001.

[17] M. Hichem and B. Tahar, "Fuzzy monitoring of stator and rotor winding faults for DFIG used in wind energy conversion system," *Int. J. Model. Identif. Control*, vol. 27, no. 1, pp. 49–57, 2017, doi: 10.1504/IJMIC.2017.082485.

[18] Z. Yang and Y. Chai, "A survey of fault diagnosis for onshore grid-connected converter in wind energy conversion systems," *Renew. Sustain. Energy Rev.*, vol. 66, pp. 345–359, 2016, doi: 10.1016/j.rser.2016.08.006.

[19] W. Qiao and D. Lu, "A Survey on Wind Turbine Condition Monitoring and Fault Diagnosis—Part I: Components and Subsystems," *IEEE Trans. Ind. Electron.*, vol. 62, no. 10, pp. 6536–6545, Oct. 2015, doi: 10.1109/TIE.2015.2422112.

[20] A. M. Patel and J. J. Patel, "PMSG with Inverter using Park ' s Transformation for Transient Fault Analysis," *IJSRD - Int. J. Sci. Res. Dev.*, vol. 3, no. 3, pp. 1713–1717, 2015.

[21] N. G. Mishra and A. A. Shaikh, " Simulation of Active and Reactive Power Control of DFIG," no. 04, pp. 76–83, 2014.

[22] N. J. Myrent, D. E. Adams, and D. T. Todd Griffith, "Aerodynamic sensitivity analysis of rotor imbalance and shear web disbond detection strategies for offshore structural health prognostics management of wind turbine blades," *32nd ASME Wind Energy Symp.*, 2014, doi: 10.2514/6.2014-0714.

[23] D. Yun and H. C. Lim, "Study of Damage Monitoring System on Wind Turbine Blades," *2013 world Congr. Adv. Struct. Eng. Mech.*, pp. 3549–3565, 2013.

[24] J. Ivanqui, H. Voltolini, R. Carlson, and E. H. Watanabe, "'Pq theory' control applied to wind turbine trapezoidal PMSG under symmetrical fault," *Proc. 2013 IEEE Int. Electr. Mach. Drives Conf. IEMDC 2013*, pp. 534–540, 2013, doi: 10.1109/IEMDC.2013.6556147.

[25] A. Kusiak and A. Verma, "A data-mining approach to monitoring wind turbines," *IEEE Trans. Sustain. Energy*, vol. 3, no. 1, pp. 150–157, 2012, doi: 10.1109/TSTE.2011.2163177.

[26] J. Niebsch, R. Ramlau, and T. T. Nguyen, "Mass and Aerodynamic imbalance estimates of wind turbines," *Energies*, vol. 3, no. 4, pp. 696–710, 2010, doi: 10.3390/en3040696.

[27] Y. Amirat, V. Choqueuse, M. E. H. Benbouzid, and J. F. Charpentier, "Bearing fault detection in DFIG-based wind turbines using the first intrinsic mode function," *19th Int. Conf. Electr. Mach. ICEM 2010*, 2010, doi: 10.1109/ICELMACH.2010.5608066.

[28] P. Li, W. Hu, R. Hu, and Z. Chen, "Imbalance fault detection based on the integrated analysis strategy for variable-speed wind turbines," *Int. J. Electr. Power Energy Syst.*, vol. 116, p. 105570, Mar. 2020, doi: 10.1016/j.ijepes.2019.105570.

BIOGRAPHIES OF AUTHORS

Vivek Kushwaha received his B.E. degree in Electrical Engineering from Gyan Ganga Institute of Technology and Sciences, Jabalpur and receives M.E. Degree in Control System from Jabalpur Engineering College, Jabalpur. His research area is control system, grid integration with renewable energy sources, especially wind turbines, and fault diagnosis in DFIG wind turbine'. He can be contacted at email: vivekkushwaha@ggits.org.

Dr. Arvind Kumar Yadav received his B.Tech. degree in Electrical Engineering from the Himachal Pradesh University (HPU), India, in 2007, the M.E. degree in Power Electronics and Drives from the Punjab Engineering College (PEC), Chandigarh, India, in 2013 and Ph.D. degree in Electrical Engineering from the GLA University, Mathura, India in 2021. He is currently in GLA University as an assistant professor since 2013. His research interest includes power electronics converters, electric drives, grid integration technologies, and application of power electronics in sustainable renewable energy. He can be contacted at email: arvind.yadav@gla.ac.in.

Dr. Sanjay Kumar Maurya currently working as an Associate Professor in the Department of Electrical Engineering, GLA University, Mathura, India. He received his Ph.D. and M.Tech. degree from MNIT Allahabad, U.P. India. He has completed his B.Sc. (Engg.) in Electrical Engineering from D E I (Deemed University), Agra, U.P. His area of interest is multi-stage distribution system planning, hybrid electric vehicle, power electronics, and renewable energy. He can be contacted at email: sanjay.maurya@gla.ac.in.